Available online at www.sciencedirect.com
SCIENCE DIRECT®
ELSEVIER Applied Mathematics and Computation 162 (2005) 707–722
APPLIED MATHEMATICS AND COMPUTATION
www.elsevier.com/locate/amc

Three-dimensional finite element analysis of soil interaction with a rigid wheel

R.C. Chiroux [a], W.A. Foster Jr. [a,*], C.E. Johnson [b], S.A. Shoop [c], R.L. Raper [d]

[a] *Aerospace Engineering Department, Auburn University, Alabama, 36849, USA*
[b] *Agricultural Engineering Department, Auburn University, Alabama, 36849, USA*
[c] *Cold Regions Research and Engineering Laboratory, Hanover, New Hampshire, 03755, USA*
[d] *National Soils Dynamic Laboratory, Auburn, Alabama, 36830, USA*

1. Introduction

Finite element analysis (FEM) has been utilized for many applications in engineering. Early applications of FEM were primarily focused on linear elastic materials. However, FEM has increasingly been utilized to analyze non-linear, non-elastic materials such as soil [1]. These applications have tended to focus on static solutions such as earthen dams and other stationary three-dimensional soil-based structures. More recently FEM has been used in non-linear, soil dynamic applications [2].

Unlike metals, soils have very little tensile strength. When compressed, they yield and become permanently deformed. These tendencies make any modeling effort including soil interaction non-linear [3–6]. Non-linear problems typically require the use of large numbers of finite elements which produce very long computational times.

Specifically, several agricultural, construction and military applications may require FEM to simulate the three-dimensional, non-linear interactions between a vehicle and the soil it traverses. These applications presently rely heavily on build and test design methods. Successful simulation would provide the opportunity for significant cost reduction in the design process.

This paper focuses on the contact and interaction between a wheel and the soil it is moving over. Up to this point, stable solutions were typically obtained

* Corresponding author.
E-mail address: wfoster@eng.auburn.edu (W.A. Foster Jr.).

0096-3003/$ - see front matter
doi:10.1016/j.amc.2004.01.013

by giving the wheel an enforced displacement with a plane strain model [7]. The objective of this effort has been threefold. First the enforced displacement constraint has been removed and the force due to the dynamic load on the wheel was applied to the model. Secondly, this effort has demonstrated the ability to accurately model this application within the limits of an engineering workstation environment. Additionally, a dynamic analysis as opposed to a static analysis provided a time history of the wheel/soil interaction and modeled the truly dynamic behavior of the problem.

2. Model description

A three-dimensional soil compaction model was constructed using the ABAQUS finite element program. Furthermore the "Explicit" version of ABAQUS was utilized rather than the "Standard" version, due to anticipated complexities and execution time. Utilization of ABAQUS/Explicit will provide further enhancement in the future by allowing both the soil and the wheel to be flexible.

This model was separated into two distinct bodies, a soil-bed and a rigid, rotating wheel. The analysis assumed symmetry about a plane normal to the wheel's rotational axis through the center of the footprint. Therefore only half of the system, as shown in Fig. 1, was modeled with the plane of symmetry in the x–z plane. Negative x was in the direction of the wheel's forward motion, positive z was vertical, normal to the soil-bed surface and positive y was from the plane of symmetry outward and was the axis about which the wheel rolled.

2.1. Soil

The main section of the soil was 7.2 m in length, 0.5 m height and 1.0 m in width. An overall view of the model is provided in Fig. 1. The longitudinal

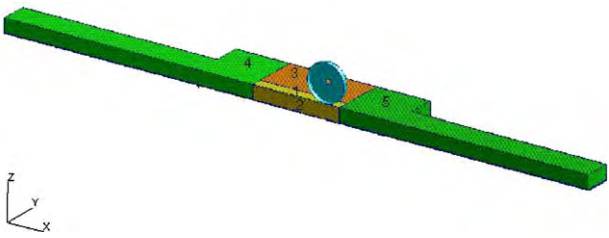

Fig. 1. Soil model including wheel.

dimension of 7.2 m represents wheel travel of approximately 1/2 of a rotation along the center third of the model, roughly 2.4 m. The model height of 1/2 m was prescribed to conform to earlier analyses and previous tests in which 1/2 m of tilled soil laid above a stiff hardpan. The width of 1.0 m was chosen to allow sufficient room beyond the edge of the wheel to reach a region where soil model response was minimal.

The soil model consisted of five distinct regions, shown in Fig. 1, each with a different mesh density, tied together by surface contacts. This approach allowed a relatively fine mesh density in the first 5 cm of soil directly under the wheel and coarser mesh densities elsewhere without complicated regions of element size transition. As a result of this approach the number of elements in the soil model was minimized which in turn minimized storage requirements and run time.

Region one was located directly below the rigid wheel and consisted of 160 elements along the length, from 2.0 to 5.2 m, two elements through the depth, from 0.45 to 0.5 m, and 20 elements across the width, from 0.0 to 0.4 m. Region two was located directly below region one and consisted of 80 elements along the length, from 2.0 to 5.2 m, nine elements through the depth, from 0.0 to 0.45 m, and 10 elements across the width, from 0.0 to 0.4 m.

Region three was located outboard of regions one and two, from 0.4 m from the x–z plane of symmetry described above to 1.0 m and consisted of 40 elements along the length, from 2.0 to 5.2 m, 10 elements through the depth, from 0.0 to 0.5 m, and six elements across the width, from 0.4 to 1.0 m. Additionally region three included infinite boundary elements attached outboard of the solid elements. There were 40 of these elements along the length, from 2.0 to 5.2 m, 10 elements through the depth, from 0.0 to 0.5 m and one element across the width, from 1.0 to 2.0 m.

Region four was located to the left of regions one, two and three and consisted of 11 elements along the length, from 0.0 to 2.0 m, six elements through the depth, from 0.0 to 0.5 m, and 11 elements across the width, from 0.0 to 1.0 m. Additionally region four included two sets of infinite boundary elements. The first set consisted of 11 elements along the length, from 0.0 to 2.0 m, six elements through the depth, from 0.0 to 0.5 m, and one element across the width, from 1.0 to 2.0 m. The second set consisted of one element along the length, from −7.2 to 0.0 m, six elements through the depth, from 0.0 to 0.5 m, and 11 elements across the width, from 0.0 to 1.0 m.

Region five was similar to region four but was located to the right of regions one, two and three and consisted of 11 elements along the length, from 5.2 to 7.2 m, six elements through the depth, from 0.0 to 0.5 m, and 11 elements across the width, from 0.0 to 1.0 m. Region five also included two sets of infinite boundary elements. The first set consisted of 11 elements along the length, from 5.2 to 7.2 m, six elements through the depth, from 0.0 to 0.5 m, and one element across the width, from 1.0 to 2.0 m. The second set consisted

of one element along the length, from 7.2 to 14.2 m, six elements through the depth, from 0.0 to 0.5 m, and 11 elements across the width, from 0.0 to 1.0 m.

The elements selected for the soil were "C3D8R", 3D, 8-node, solid elements. This element supports only the three translation degrees of freedom in the x, y and z directions. The C3D8R uses reduced integration, which greatly reduces computation time at the expense of element stability. Infinite element stability was not critical as the model was designed for minimal soil-bed model activity in these regions. Hourglass control, integral to these elements, provides artificial stiffening against element instability.

The attached infinite elements were "CIN3D8", 3D, 8-node, one-way infinite solid elements. These elements match the main body and were oriented so as to extend the model's mathematical length to plus and minus infinity and width to plus infinity. The shape and orientation of this element are similar to the C3D8R element above except that the element must be attached such that the infinite end faces away from the model. Infinite elements are beneficial as energy is dissipated at model edges rather than reflected back into the structure. Infinite elements are allowed only linear, elastic behavior so they must be positioned a sufficient distance from the non-linear wheel/soil interaction region to ensure accuracy.

2.2. Rigid, rotating wheel

The rigid wheel was 1.372 m in diameter (54 in.), 1524 m width (6 in.) and was modeled with "R3D4" rigid 3D elements. 72 rigid elements in all were used along the wheel perimeter, each element covering 5°, and were attached to a reference node at the radial center of the wheel. Due to the use of reflective symmetry only half the wheel was modeled. This model represented a wheel that was. 3048 m (12 in.) in width. Additionally, this placed the rigid body reference node on the plane of symmetry. In addition to the perimeter elements 72 additional rigid elements, acting as a sidewall, were attached to the outer edge of the wheel ($y = 0.1524$ m) extending radially inwards 0.6 m with a slight cant outward ($y = 0.1530$ m). The purpose of these sidewall elements was for model stability. The rigid wheel is depicted in Fig. 2.

The initial position of the wheel was located such that the radial center was near one edge of the center third of the soil ($x = 4.68$ m). The radial center was positioned vertically such that the perimeter of the rigid wheel just touched the surface of the soil. This initial positioning allowed the wheel to initially settle into the soil and then roll counter-clockwise for approximately 1/2 rotation along the center third of the soil (approximately 2.16 m).

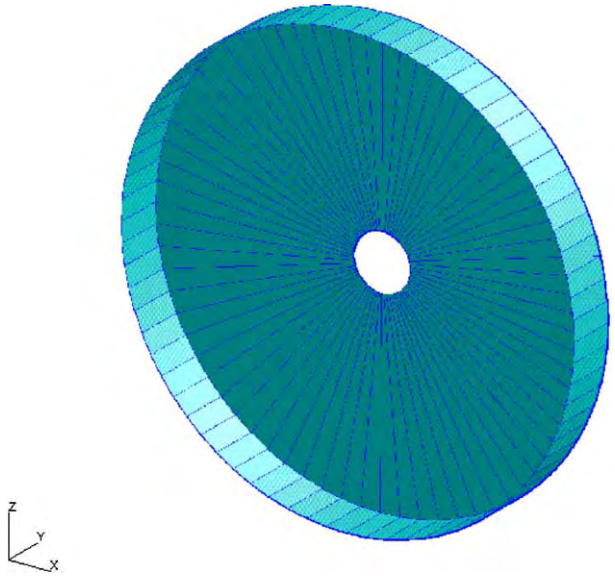

Fig. 2. Rigid wheel.

3. Material property description

3.1. Soil

The material properties of the soil were based on data for ''Norfolk Sandy Loam'' as defined by Block [8]. The density (ρ) of the soil was 1255.2 kg/m^3, the initial elastic modulus (E) was 326.2 kPa and initial Poisson's ratio (v) was 0.00. The infinite elements utilized the same material properties. This initial elastic modulus increased with compaction due to hardening. The value of Poisson's ratio was also modified model during the analysis. The prescribed initial yield stress level was assumed to be 0 kPa for the tilled soil at the surface.

The soil was modeled using the ''cap plasticity'' and ''cap hardening'' options within ABAQUS/Explicit. These options enabled plastic deformations to commence at a prescribed stress level and included Drucker–Prager hardening. Additionally each layer of soil elements was given an initial volumetric plastic strain corresponding to the hydrostatic pressure induced due to the weight of the soil above that layer. This simulated an initial state of compaction for soil elements below the model surface. Additional initial compaction due to air pressure was discounted on the assumption that tilled soil is unable to develop a pressure gradient.

Within the ''cap plasticity'' option of ABAQUS/Explicit three additional parameters, material cohesion (d), material angle of friction in the p–q plane

Table 1
Cap hardening stress/strain curve

Hydrostatic yield stress (kPa)	Volumetric plastic strain	Hydrostatic yield stress (kPa)	Volumetric plastic strain
0	0	80	0.149679
5	0.014661	90	0.160028
10	0.028334	100	0.169280
20	0.053024	120	0.185036
30	0.074619	160	0.208422
40	0.093572	210	0.228045
50	0.110262	290	0.248232
60	0.125006	400	0.266976
70	0.138069	500	0.280999

(β) and a cap eccentricity parameter (R) were required. Material angle of friction was defined to be 57.8° for Norfolk Sandy Loam [9]. Cohesion was defined as 350 Pa and cap eccentricity 0.0005. Cap plasticity and cap eccentricity values were determined from considerable trial runs to optimize model performance to test data from Block [8].

The stress–strain curve utilized was a piecewise linear approximation derived from experimental data and is shown in Table 1. The data available for hydrostatic pressure yield stress vs. volumetric plastic strain, was limited to a hydrostatic pressure yield stress range from 5 to 500 kPa.

3.2. Rigid, rotating wheel

A rigid wheel, modeled by ABAQUS/Explicit, can have a weight assigned to it by one of two means: A concentrated load at the center of the wheel, specifically the reference node, or via concentrated mass elements attached along the perimeter of the wheel. The latter option was utilized in this case as it appeared to give a better simulation of the weight distribution of the wheel. The latter method is not identified by the ABAQUS/Explicit manual directly, but does provide a valid means of applying weight to a rigid body.

Concentrated mass elements of 4.1057878 kg were attached at each of the nodes along the perimeter of the rigid wheel in contact with the reflective plane of symmetry. This translated to 295.617 kg total. As will be mentioned later, this mass, in combination with a 1 g acceleration, yielded a rigid wheel weight of 2.9 kN, half of the total dynamic rigid wheel load of 5.8 kN. The wheel loading of 11.6 kN was achieved in a similar manner.

4. Boundary conditions

In order to properly model the dynamic interaction between the soil and rigid rotating wheel various boundary and loading conditions were utilized.

These boundary conditions were functionally divided into conditions that affect the soil model, that affect the rigid wheel and those that define the interaction between the soil and rigid wheel.

4.1. Soil

The base of the soil was fully constrained in all three translational degrees of freedom (''*x*'', ''*y*'', ''*z*''). The intent was to model untilled, compacted soil beneath 0.5 m of loose, tilled soil. All nodes along the longitudinal centerline of the model, or reflective plane of symmetry, were given the ''YSYMM'' boundary condition. This translated to fully constraining ''*y*'' displacement and rotation about the ''*x*'' and ''*z*'' axes. As noted above, the longitudinal and outboard ends of the soil were terminated with infinite elements to match boundary conditions at infinity. The surface of the soil was not constrained.

4.2. Rigid, rotating wheel

The rigid wheel had two enforced constraints, a gravitational acceleration and a rotation. These are discussed further under loading conditions.

4.3. Interaction between the soil and rigid, rotating wheel

Two surfaces were defined to properly connect the rigid wheel to the soil. One surface was defined along the top edge of the soil and another along the outer surface of the rigid wheel. The surfaces were then defined relative to each other by declaring them a ''contact pair''. This technique allowed the surfaces of the two separate, distinct bodies of the model to come in contact but not to cross each other. This in turn allowed the rigid wheel to load the soil as gravitational acceleration was gradually applied to the wheel.

A typical friction interaction coefficient of 0.6 was also defined between the two surfaces. This allowed the rigid wheel to achieve traction on the surface of the soil when the wheel began its counter-clockwise roll.

5. Loading environment

For both the 5.8 and 11.6 kN loading conditions, the analysis was divided into 12 time steps. The number of time steps chosen was limited by available disk storage considerations. In both conditions the first 5 time steps were 1 s in duration and applied a linearly ramped acceleration from 0 to 9.81 m/s^2 to each of the concentrated mass elements. This approach allowed the rigid wheel to gradually load the soil to avoid simulating an impact and to minimize oscillations. As a result of a series of trial runs, 5.0 s was determined to be the

minimum acceleration ramp time needed to bring the rigid wheel to a stable starting position in the soil before rolling commenced. During all subsequent time steps the acceleration was held constant.

For both cases the sixth time step was utilized to linearly ramp the rotational velocity of the rigid wheel from 0 to its maximum. The duration of this time step was also 1 s. The 5.8 kN case was ramped to a positive, counter-clockwise rotational velocity of 0.244 rad/s while the 11.6 kN case was ramped to 0.269 rad/s. These rotational velocities correspond to translational velocities of 16.74 cm/sec (0.374 mph) and 18.45 cm/sec (0.413 mph) respectively. These velocities were chosen to correspond with earlier test data (Block, 1991). These velocities were held constant during all subsequent time steps.

In both cases the seventh through twelfth time steps were utilized to roll the rigid wheel approximately 1/2 of a revolution. For the 5.8 kN case this required approximately 12 s and approximately 11 s for the 11.6 kN case. To achieve this the 5.8 kN case consisted of 6 time steps of 2 s duration each while the 11.6 kN case consisted of five time steps of 2 s duration each followed by 1 time step of 1 s duration.

6. Results

The primary objectives were to achieve displacement and stress results analytically and compare these to previously acquired experimental laboratory test data for a rigid wheel [7,8]. Accordingly, analytical results reviewed in this paper were focused on soil compaction wheel rut depth, octahedral normal stress and octahedral shear stress. Three locations were reviewed for stress comparisons. Location 1 was located at 30 cm depth below the wheel centerline, location 2 was 30 cm depth below the wheel edge and location 3 was 15 cm depth below the wheel centerline. The test data referred to above is presented in Table 2.

When comparing test data to analytical results, several issues must be considered. The test data reported peak values of octahedral normal and shear stress. It appears that these values were calculated from peak values of the principle stresses, which did not necessarily occur at the same physical location. Thus the octahedral normal and shear stresses reported would represent a composite value based on the peak principle stresses. The values reported in the finite element model represent values at specific locations in the soil. Also, the measured peak stresses occurred ahead of the wheel centerline, as opposed to directly below the wheel centerline. In addition, the pressure transducers used during the tests had a maximum dimension between 6 and 8 cm. Considering rut depths of 11 to 15 cm for the 5.8 and 11.6 kN loads, respectively, the transducer size possibly introduced some stiffening to the soil-bed. Finally, the

Table 2
Experimental test data

Wheel load (kN)	Location	Rut depth (cm)	Peak octahedral normal stress range (kPa)		Peak octahedral shear stress range (kPa)	
			Min.	Max.	Min.	Max.
5.8		10.88				
	1		11.0	31.1	18.0	63.4
	2		8.0	18.4	19.3	24.4
	3		16.3	34.1	24.0	51.9
11.6		15.25				
	1		86.0	112.2	108.0	135.8
	2		22.1	76.6	29.8	112.0
	3		78.6	214.1	90.9	241.3

test data presented for comparison included a 10% slip while the analytical results assumed 0 slip.

The analytical results are presented in a series of figures and summarized in Table 3. All stress results presented in Table 3 are at an elapsed time of 12 s and are values directly under the wheel hub. Rut depths listed are steady state depths after the rigid wheel has passed. Location 2, rigid wheel edge, is at a lateral location of $y = 0.16$ cm.

The following series of figures present 3-D deformation results along the wheel centerline, x–z plane of symmetry, from an elapsed time of 5 to 16 s. The elapsed time represents a counter-clockwise wheel roll of approximately 1/2 of a rotation at a steady state wheel loading of 1 g. Figs. 3 and 4 present a 3-D shaded image of rut formation for a wheel load of 5.8 and 11.6 kN, respectively. Figs. 5 and 6 present a 3-D contour image of vertical deformations to the soil-bed for a wheel load of 5.8 and 11.6 kN, respectively.

Table 3
Finite element results

Wheel load (kN)	Location	Rut depth (cm)	Octahedral normal stress (kPa)	Octahedral shear stress (kPa)
5.8		10.10		
	1		14.5	11.0
	2		7.0	5.4
	3		17.0	12.8
11.6		16.50		
	1		27.5	20.5
	2		7.9	6.1
	3		31.0	23.0

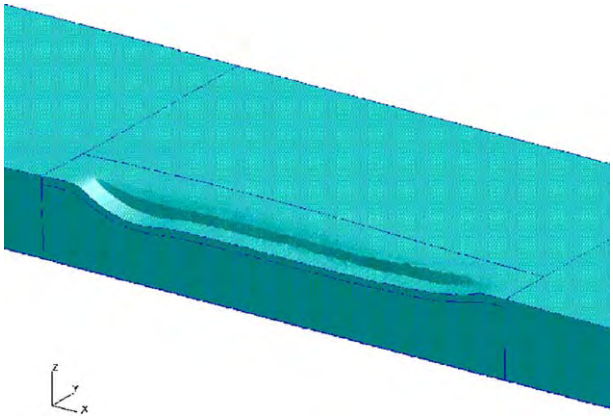

Fig. 3. 5.8 kN load, elapsed time = 16 s, rut formation.

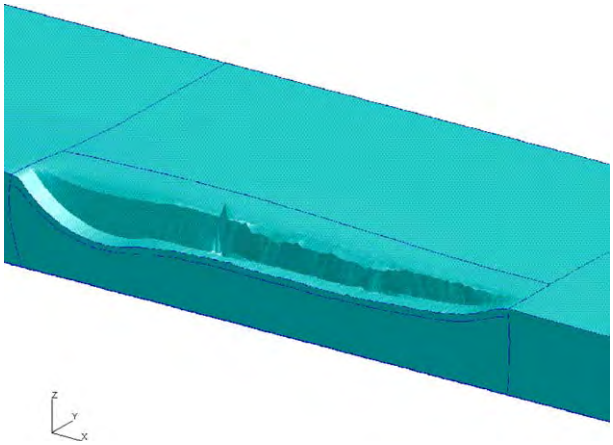

Fig. 4. 11.6 kN load, elapsed time = 16 s, rut formation.

The next series of figures present vertical deformations, octahedral normal and shear stresses along sections in the x–z plane outward from the x–z plane of symmetry. The purpose of these figures is to illustrate the three-dimensional response of the soil to the load imposed by the rolling wheel. The section at which $y = 0.16$ cm is equivalent to the wheel edge, $y = 0.32$ cm is equivalent to an additional 1/2 wheel width outboard of the wheel edge and $y = 0.60$ cm is equivalent to 1.5 times the wheel width outboard from the wheel edge. All figures are for an elapsed time of 12 s which corresponds to approximately 1/2 of the total wheel roll. Figs. 7–10 present a 3-D contour image of vertical deformations to the soil-bed, from the wheel centerline to $y = 0.60$ cm, at an

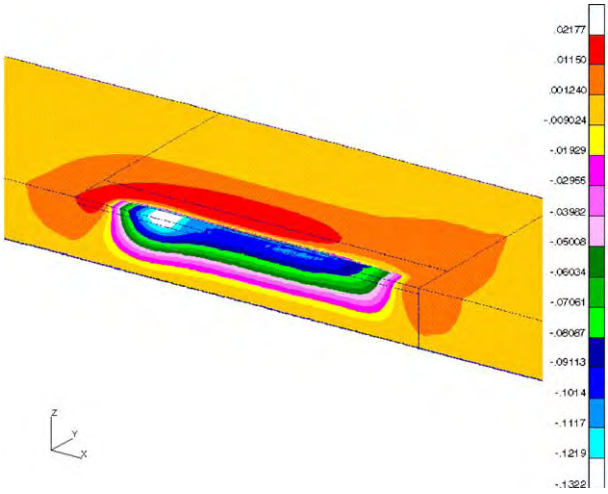

Fig. 5. 5.8 kN load, elapsed time = 16 s, vertical deformation.

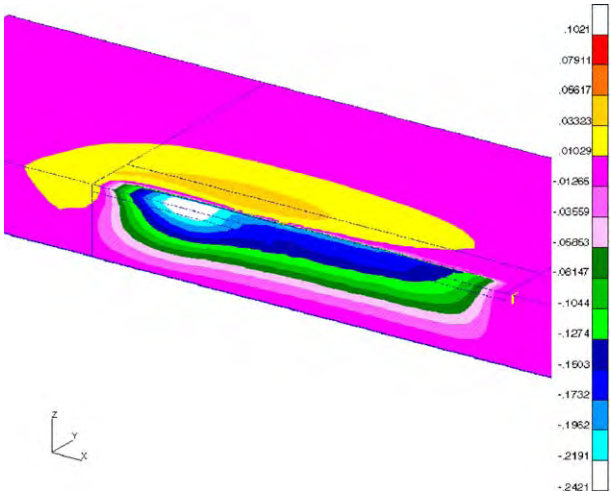

Fig. 6. 11.6 kN load, elapsed time = 16 s, vertical deformation.

elapsed time of 12 s and a wheel load of 5.8 kN. Figs. 11 and 12 present a 3-D contour image of octahedral normal stress to the soil-bed, at the wheel centerline and $y = 0.60$ cm, at an elapsed time of 12 s and a wheel load of 5.8 kN. Figs. 13 and 14 present a 3-D contour images of octahedral shear stress to the soil-bed, at the wheel centerline and $y = 0.60$ cm, at an elapsed time of 12 s and a wheel load of 5.8 kN.

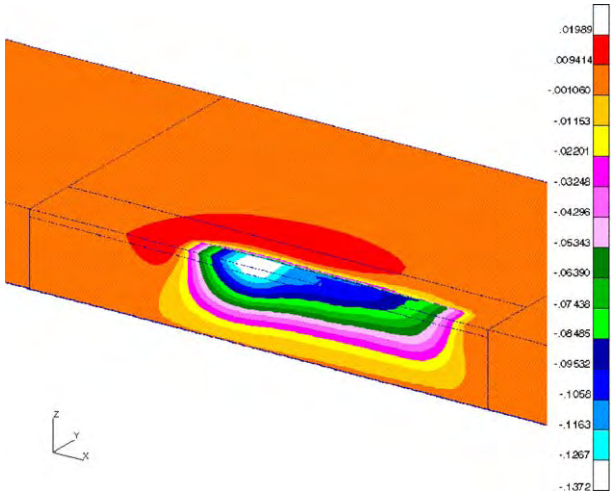

Fig. 7. 5.8 kN load, elapsed time = 12 s, vertical deformation, centerline.

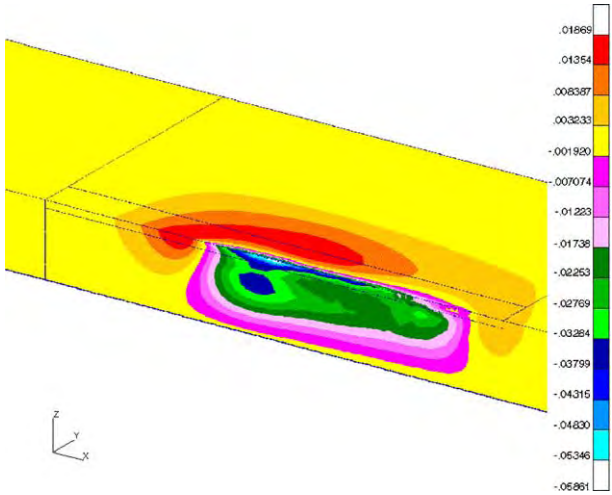

Fig. 8. 5.8 kN load, elapsed time = 12 s, vertical deflection, $y = 0.16$ cm.

7. Conclusions

This effort has been successful in producing a 3D finite element model, within the limits of an engineering workstation, that reasonably predicts soil response to a dynamically loaded rolling wheel following a straight line path.

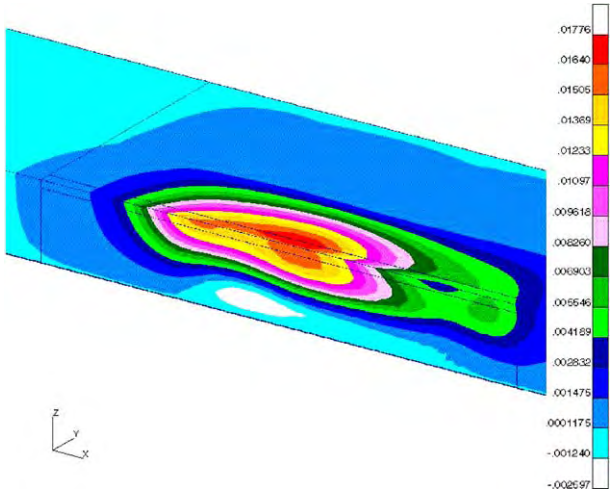

Fig. 9. 5.8 kN load, elapsed time = 12 s, vertical deformation, $y = 0.32$ cm.

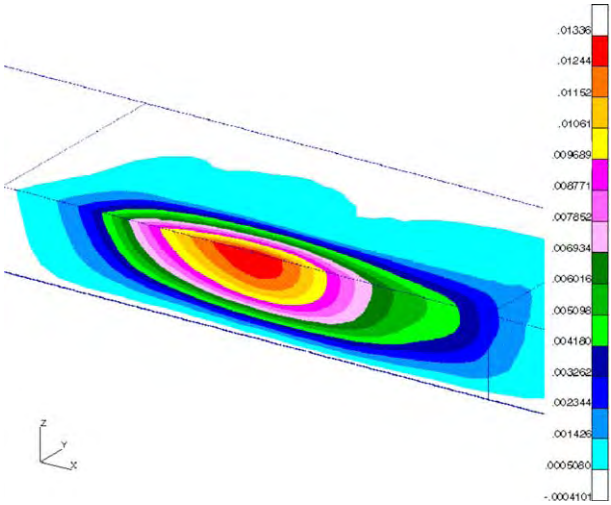

Fig. 10. 5.8 kN load, elapsed time = 12 s, vertical deformation, $y = 0.60$ cm.

Of greatest concern is the tendency of the soil to rebound, to some degree, after passage of the wheel. This rebound appears to be on the order of 25% of the total deflection. This rebound is not seen experimentally. Considerable effort was made to vary the Drucker–Prager soil model parameters to minimize this effect without much success.

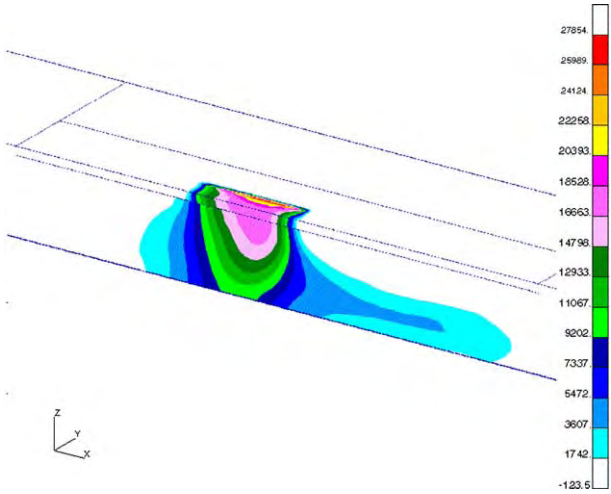

Fig. 11. 5.8 kN load, elapsed time = 12 s, octahedral normal stress, centerline.

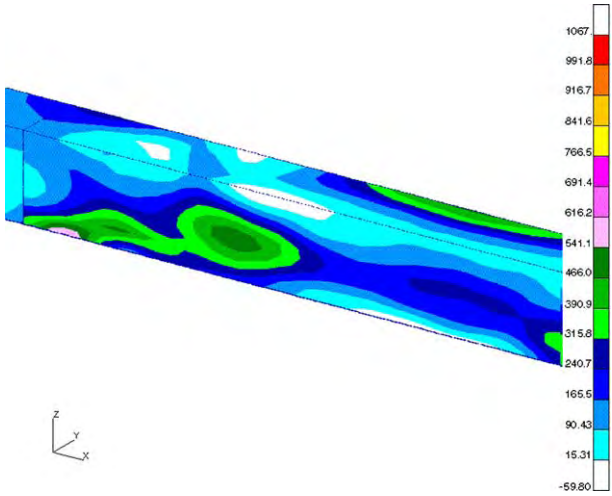

Fig. 12. 5.8 kN load, elapsed time = 12 s, octahedral normal stress, $y = 0.60$ cm.

In spite of the rebound, the resulting deflections after the wheel passage do agree rather well with the experimental data. Stress results also agree rather well with the experimental data when consideration is given concerning comparison of analytical stress under the wheel hub to experimental peak stresses at other locations, slip and the presence of relatively large, stiff pressure transducers buried in the soil during experimental data acquisition.

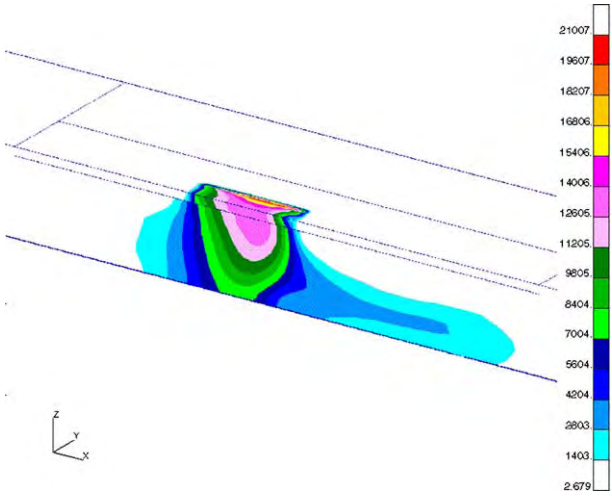

Fig. 13. 5.8 kN load, elapsed time = 12 s, octahedral normal stress, centerline.

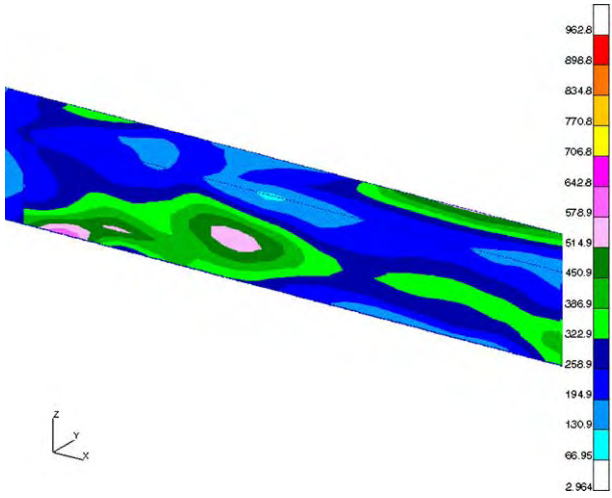

Fig. 14. 5.8 kN load, elapsed time = 12 s, octahedral shear stress, $y = 0.60$ cm.

References

[1] G.J. Dvorak, R.T. Shield, Mechanics of Material Behavior, Elsevier Science Publishing Company, Inc., New York, NY, 1984.
[2] Z.P. Bazant, Mechanics of Geomaterials, Rocks, Concretes, Soils, John Wiley & Sons Inc., New York, NY, 1985.

[3] A.C. Bailey, G.E. Vanden Burg, Yielding by compaction and shear in unsaturated soils, Transactions of the ASAE 11 (3) (1968) 307–311, 317.
[4] A.C. Bailey, C.E. Johnson, R.L. Schafer, Hydrostatic compaction of agricultural soils, Transactions of the ASAE 27 (4) (1984) 952–955.
[5] A.C. Bailey, C.E. Johnson, R.L. Schafer, A model for agricultural soil compaction, Journal of Agricultural Engineering Research 33 (1986) 257–262.
[6] A.C. Bailey, C.E. Johnson, Soil Compaction, Auburn University, Auburn, AL, 1996.
[7] W.A. Foster Jr., C.E. Johnson, R.L. Raper, S.A. Shoop, Soil deformation and stress analysis under a rolling wheel, in: Proceedings of the 5th North American ISTVS Conference/Workshop, Saskatoon, SK, Canada. 10–12 May, 1995.
[8] W.A. Block, Analysis of soil stress under rigid wheel loading, Unpublished Ph.D. Dissertation, Auburn University, Auburn, AL, 1991.